FULL PAPER

Tissue Engineering

ADVANCED
HEALTHCARE
MATERIALS

www.advhealthmat.de

Melt Electrospinning Writing of Poly-Hydroxymethylglycolide-co-ε-Caprolactone-Based Scaffolds for Cardiac Tissue Engineering

Miguel Castilho,* Dries Feyen, María Flandes-Iparraguirre, Gernot Hochleitner, Jürgen Groll, Pieter A. F. Doevendans, Tina Vermonden, Keita Ito, Joost P. G. Sluijter,* and Jos Malda*

Current limitations in cardiac tissue engineering revolve around the inability to fully recapitulate the structural organization and mechanical environment of native cardiac tissue. This study aims at developing organized ultrafine fiber scaffolds with improved biocompatibility and architecture in comparison to the traditional fiber scaffolds obtained by solution electrospinning. This is achieved by combining the additive manufacturing of a hydroxyl-functionalized polyester, (poly(hydroxymethylglycolide-co-ε-caprolactone) (pHMGCL), with melt electrospinning writing (MEW). The use of pHMGCL with MEW vastly improves the cellular response to the mechanical anisotropy. Cardiac progenitor cells (CPCs) are able to align more efficiently along the preferential direction of the melt electrospun pHMGCL fiber scaffolds in comparison to electrospun poly(ε-caprolactone)-based scaffolds. Overall, this study describes for the first time that highly ordered microfiber (4.0–7.0 µm) scaffolds based on pHMGCL can be reproducibly generated with MEW and that these scaffolds can support and guide the growth of CPCs and thereby potentially enhance their therapeutic potential.

1. Introduction

Heart failure is a debilitating disease for patients and is often associated with a poor quality of life, as well as high morbidity and mortality.[1] The heart is hardly able to repair after cardiac injury (e.g., due to myocardial infraction) and is often associated with progressive pathological remodeling to compensate for contractility loss.[1] Current clinical therapies for heart failure do not treat the underlying loss of myocardial tissue and thereby do not halt the progression of the disease. Therefore, regenerative therapies that involve stem or progenitor cells have been proposed as potential future approaches.[2] Biomaterials have been suggested to be essential and useful as critical regulators of the organization of stem cells for cardiac tissue engineering (TE) applications.[3] Nonetheless, recreating native cardiac tissue in vitro still remains a major challenge.[4,5] Despite the great potential of 3D biofabrication to accurately deposit cells and biomaterials together into desired geometries,[6] these techniques are currently unable to fully address the needed structural fiber organization and mechanical environment of endogenous cardiac tissue.

In that respect, embedding cardiac progenitor cells (CPCs) into fiber-based scaffolds is a promising approach as the fiber

Dr. M. Castilho, M. Flandes-Iparraguirre, Prof. K. Ito, Prof. J. Malda
Department of Orthopaedics
University Medical Center Utrecht
P.O. Box 85500, Utrecht, GA 3508, The Netherlands
E-mail: m.diascastilho@umcutrecht.nl; j.malda@umcutrecht.nl

Dr. M. Castilho, Prof. K. Ito
Department of Biomedical Engineering
Eindhoven University of Technology
P. O. Box 513, Eindhoven, MB 5600, The Netherlands

Dr. M. Castilho, Dr. D. Feyen, M. Flandes-Iparraguirre,
Prof. J. P. G. Sluijter, Prof. J. Malda
Regenerative Medicine Center Utrecht
Uppsalalaan 8, Utrecht, CT 3584, The Netherlands
E-mail: j.sluijter@umcutrecht.nl

Dr. D. Feyen, M. Flandes-Iparraguirre, Prof. P. A. F. Doevendans,
Prof. J. P. G. Sluijter
Department of Cardiology
Experimental Cardiology Laboratory
University Medical Center Utrecht
P.O. Box 85500, Utrecht, GA 3508, The Netherlands

G. Hochleitner, Prof. J. Groll
Department of Functional Materials in Medicine and Dentistry
and Bavarian Polymer Institute
University of Würzburg
Pleicherwall 2, Würzburg 97070, Germany

Dr. T. Vermonden
Department of Pharmaceutics
Utrecht Institute for Pharmaceutical Sciences (UIPS)
Utrecht University
P. O. Box 80082, Utrecht, TB 3508, The Netherlands

Prof. J. Malda
Department of Equine Sciences
Faculty of Veterinary Medicine
Utrecht University
Utrecht, 3584 CM, The Netherlands

**ADVANCED
SCIENCE NEWS**

www.advancedsciencenews.com

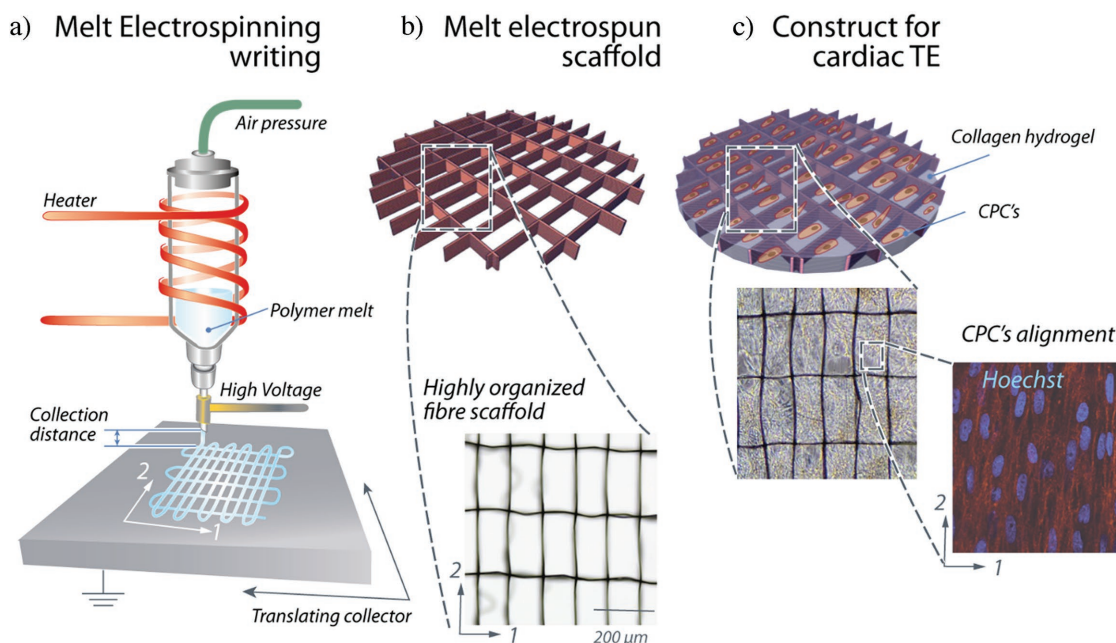**ADVANCED
HEALTHCARE
MATERIALS**

www.advhealthmat.de

Figure 1. a) Schematic of the custom-built MEW device and its principal components: Dispensing unit assisted by air-pressure; electrical heating system; HV source electrode; and computer-assisted collector plate. b) Produced melt electrospun fiber scaffolds based on pHMGCL polymer. Optical image of well-organized scaffolds architecture (microfibers $\varnothing$ = 4.0–7.0 µm) having a rectangular pattern (pore size = 150 × 300 µm). c) Fiber scaffold infiltrated with CPCs/Collagen hydrogel. Immunostaining of the rectangular scaffolds seeded after 7 d in culture, showing that the oriented fiber architecture promoted cell alignment according to the rectangular shape scaffold long axis. Nuclei, stained in blue.

network has the potential to mimic the fibrillar structure of the native extracellular matrix (ECM).[7] Among the different technologies used for fiber scaffold fabrication, electrospinning of polymer solutions is relatively popular due to its simplicity and cost-effectiveness. Recently, the potential of using electrospun fiber scaffolds of polycaprolactone (PCL)[8] or functionalized PCL to mimic the aligned ECM of the native heart muscle[9] was demonstrated. Nevertheless, the lack of biological compatibility of PCL compared to that of natural polymers necessitated postprocessing steps in order to improve cell–scaffold interactions. Moreover, despite the promising microfiber diameters obtained, appropriate fiber alignment and mechanical properties that could recreate the microenvironment of the cardiac tissue could not be achieved.

Direct melt electrospinning writing (MEW) is an additive manufacturing process that has recently emerged as an alternative polymer processing technology for fiber scaffold manufacturing.[10] This technology is based on an electro-hydrodynamic working principle to deposit fibers from polymer melts to highly defined scaffold structures. While the fiber diameters can be tailored between ≈0.8[11] and ≈140 µm[12] depending on printing conditions and polymer characteristics, the range of polymers that have been applied in MEW is still very limited, with PCL being the most commonly used.[13] However, PCL is relatively hydrophobic, degrades slowly, and is, therefore, in our opinion not regarded as the ideal material for true myocardial integration and regeneration.

In the current study, we developed ultrafine fiber scaffolds with enhanced biocompatibility and improved fiber architecture that could stimulate cell retention and guide cardiac cell growth. This was achieved by combining MEW technology with poly (hydroxymethylglycolide-co-ε-caprolactone) (pHMGCL) (**Figure 1**). This hydroxyl-functionalized polyester (pHMGCL) has increased hydrophilicity in comparison to PCL,[14,15] a tunable degradation rate, and has the potential for further functionalization.[16,17] Therefore, in this study, MEW of pHMGCL was systematically investigated in order to obtain reproducible fiber scaffolds. Different scaffold architectures were compared to assess the effect on mechanical behavior, cellular alignment, and organization. Biological relevance of the fiber scaffolds was tested with human CPCs, a promising therapeutic cell type that can be isolated directly from a patients' heart and differentiated into cardiomyocytes and vascular cells.[18]

2. Results and Discussion

2.1. MEW

2.1.1. Polymer Characterization for Melt Electrospinning

The ability to melt electrospin a polymer is mainly determined by material characteristics like molecular weight and thermal properties of the polymer.[13] In this study, two polymer formulations were used, i.e., pHMGCL, PCL, and blends of pHMGCL with PCL in two different weight ratios (i.e., 20:80—Blend20 and 40:60—Blend40; material properties are summarized in **Table 1**). Gel permeation chromatography (GPC) analysis revealed that the molecular weight of pHMGCL (M_w = 39 kDa) was substantially lower than that of

**ADVANCED
SCIENCE NEWS**

www.advancedsciencenews.com

**ADVANCED
HEALTHCARE
MATERIALS**

www.advhealthmat.de

Table 1. Characteristics of the pure polymers and blends used in this study.

Composition	M_w [kDa][a]	PDI[a]	T_g [°C][b]	T_m [°C][b]	Water contact angle [°]
PCL	71	1.9	−65.5	54.4	70.9 ± 1.5
pHMGCL	38.9	2.1	−51.6	44.5	54.2 ± 0.9
Blend20	N.A.	N.A.	−60.4	54.1	67.2 ± 1.6
Blend40	N.A.	N.A.	−59.2	54.2	58.7 ± 2.1

Measured by [a]GPC and; [b]DSC.

PCL (M_w = 71 kDa), while thermograms demonstrated a lower melting temperature of pHMGCL (T_m = 44.5 °C) when compared to PCL (T_m = 54.4 °C). By increasing the relative amount of pHMGCL from 20 to 40 wt%, the melting temperature of the blends slightly decreased in comparison with the pure PCL polymer. Hydrophilicity of the pHMGCL polymer and its blends was also confirmed by contact angle measurements, where pHMGCL had a much lower contact angle (54.2 ± 0.9°) than the PCL polymer alone (70.9 ± 1.5°), as reported previously.[14] Consistently, measured contact angles for the 20 and 40 wt% pHMGCL blends were lower than for the pure PCL (67.2 ± 1.6° and 58.7 ± 2.1°, respectively). This underscores the potential of blending the PCL with pHMGCL to reduce the intrinsic hydrophobicity of the PCL polymer, without significant modification of its thermal properties.

2.1.2. Fabrication of Melt Electrospun Scaffolds

Preliminary tests demonstrated that melt electrospinning of pHMGCL polymer resulted in a persistent noncontinuous and unstable material jet despite the similar thermal properties to PCL, hampering the adequate material collection and writing (data not shown). This was most likely due to Rayleigh instabilities and consequently formation of noncontinuous polymer jets due to the significantly lower M_w and insufficient macromolecular entanglements of this polymer compared to the PCL. On the other hand, the melt electrospinning of 20 wt% pHMGCL/PCL (Blend20) and 40 wt% pHMGCL/PCL (Blend40) yielded jets that enabled the direct writing of fibers. As a superior interaction of the CPCs was expected for the Blend40 due to the higher hydrophilicity, this blend was specifically used for further evaluation. The interdependence of fiber properties on instrument parameters was subsequently evaluated in order to establish appropriate processing conditions.

2.1.3. Investigation of Processing Parameters on Fiber Shape and Diameter

Polymer jet formation and dependency of fiber shape on the velocity of the collector plate were examined for the Blend40 and PCL formulations (**Figure 2**). Continuous jets were formed between the Taylor cone and the contact point on the translating collector plate for both polymers. A slightly lower meniscus formation was observed at the nozzle end for the Blend40, as well as a lower jet deflection, when compared to the PCL polymer (selected representative images of polymer jet formation in Figure 2). Transition of sinusoidal fibers to straight fibers occurred at higher collecting speeds for the Blend40 (25 mm s^{-1}) than for the PCL (10 mm s^{-1}). This speed is usually defined as the "critical translation speed" (CTS)[12] and defines the speed at which the collector plate matches the ultimate jet speed, which is critical for the fabrication of scaffolds with well-defined and controlled architectures (Figure 2).

Having determined the CTS for both polymer formulations, the effect of the key processing parameters, i.e., feeding pressure (p), applied voltage (U_{acc}), collecting speed (v_{col}), and collecting distance (d), on fiber diameter was systematically investigated (Figure 2c–e). By increasing the feeding pressure from 1 to 4 bar, the average diameter of the deposited fibers increased from ≈3 to 7 µm and 4 to 12 µm for the Blend40 and PCL, respectively. This increased diameter can be explained by the increase in molten polymer flow rate and was more pronounced for the PCL polymer. With the increase of the applied voltage, a jet-thinning effect was observed (Figure 2d). This phenomenon is in line with observations reported previously for fiber fabrication with both solution[19] and melt electrospinning.[20] Moreover, the diameter of the fibers decreased, regardless of polymer composition, approximately by 40% when the collector translational speed was doubled. This latter instrument parameter mostly dictates the mechanical drawing forces and, therefore, was found to also play a critical role in controlling both fiber shape and diameter. In addition, the effect of collector distance on fiber diameter was studied, but no clear effect was observed (data not shown). This might be related to the fact that only at spinning distances of 3 to 5 mm, stable jets were observed. Finally, the spinning temperatures were kept at the minimum spinning temperatures for stable printing conditions: 87 and 94 °C for Blend40 and PCL, respectively. This was higher than the determined melting temperatures (as determined by differential scanning calorimetry (DSC) analysis) due to an energy loss observed through MEW printing head and also to ensure a sufficient drop in the viscosity of the molten polymers, required to attain stable polymer jets. Thus, melt electrospinning of the Blend40 was found to require considerable higher acceleration voltages, U_{acc} = 7 kV, higher collecting speeds, V_{col} = 25 mm s^{-1}, and lower spinning temperatures, T = 84 °C, than the standard PCL polymer, in order to generate fibers with a diameter of ≈4–7 µm. The fiber diameters obtained from the pHMGCL-containing blends were close to the lowest fiber diameters typically obtained for MEW of PCL, 0.8–60 µm,[8,9,21] and one order of magnitude lower than the common extruded 3D-printed PCL scaffolds.[22] Such fiber diameters of 4–7 µm were chosen as these provide a good balance between cellular interaction and scaffold handling. With regard to optimal cell adhesion, thin fibers are often preferred due to the high specific surface area.[23] However, scaffolds with fibers below 3–5 µm were hard to handle and may be more prone to loss of their structural stability during in vivo application.

**ADVANCED
SCIENCE NEWS**
www.advancedsciencenews.com

**ADVANCED
HEALTHCARE
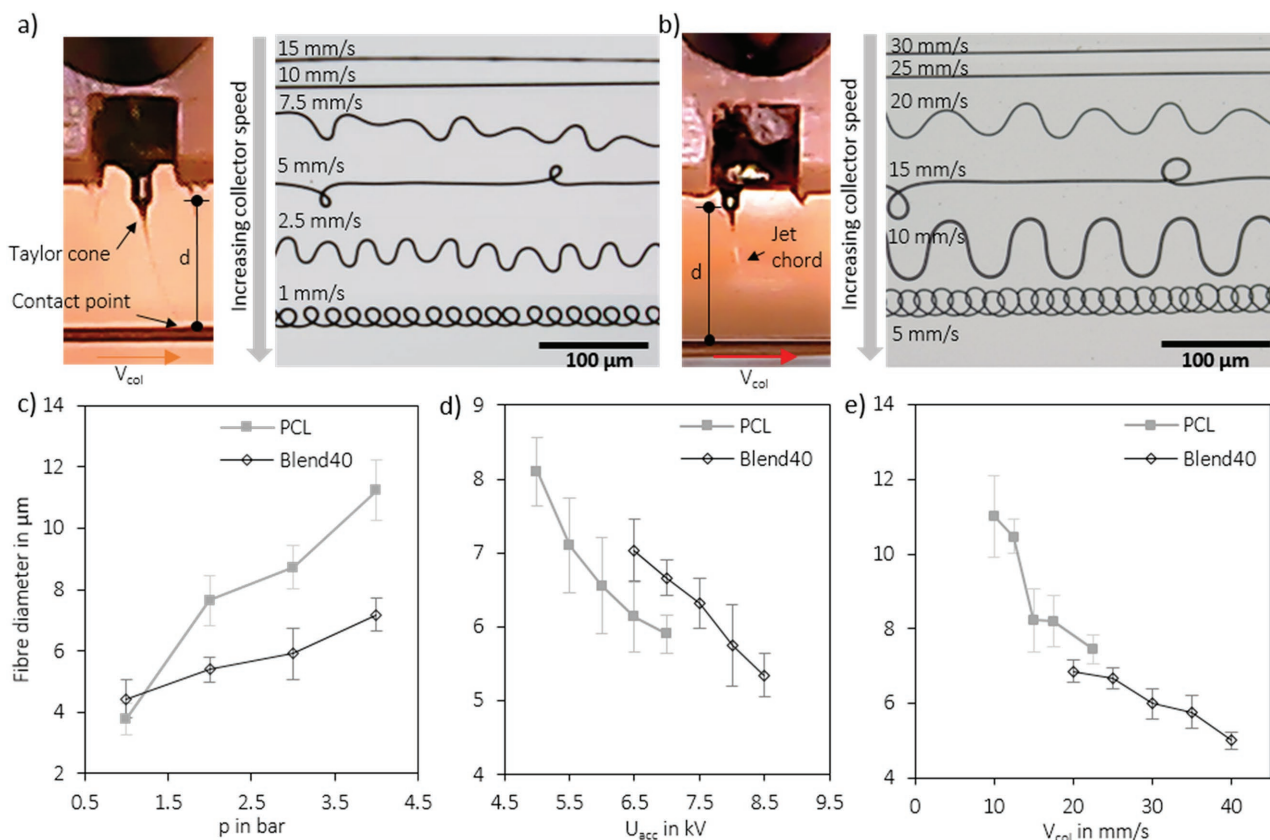MATERIALS**
www.advhealthmat.de

Figure 2. Effect of MEW key processing parameters on fiber shape, diameter, and orientation. Optical micrographs of fiber shape modification at different collector speeds for a) PCL and b) Blend40. Stable segment of fiber jet formation between the Taylor cone and contact point on the subtract is also illustrated for both polymers at the collection distance of $d = 3$ mm. Evaluation of fiber diameter as function of c) feeding pressure (p), d) acceleration voltage (U_{acc}), and e) collector velocity (v_{col}) for the collection distance represented.

2.1.4. Layer-by-Layer Deposition: Scaffold Manufacturing

In order to create coherent 3D scaffold structures with relevant pore sizes for cardiac TE, the ability to stack microfibers in a layer-by-layer fashion was evaluated. Scanning electron microscopy (SEM) analysis revealed the accurateness of the fiber stacking for the two types of scaffold geometries, i.e., rectangular and squared, from both polymers, Blend40 and PCL (**Figure 3**). Linear fibers were successfully stacked on the top of each other up to a height of 400 µm, comparable to a 3D-printed heart patch previously implanted in a murine model of myocardial infarction.[3] Furthermore, the minimum pore size (i.e., interfiber distance) was ≈±150 µm, without significant differences between the two polymer formulations. For interfiber distances below 150 µm, unstable jets were observed due to the repulsive forces generated between deposited fibers and the polymer jet.[10] Therefore, the square- and rectangular-shaped scaffolds were printed with the side dimensions of 200 µm × 200 µm and 150 µm × 300 µm, respectively. Aside from the small pore size achieved with a periodic structure, voids between adjacent fibers were observed at the edges of the box structures (arrow in Figure 3c). These pores through the walls of stacked fibers were observed for both Blend40 and PCL scaffolds and were most likely determined by the differences in

the cumulative charge of each fiber stack that repelled the subsequent layer due to an heterogeneous tensile drag.[24]

2.2. Mechanical Testing of the MEW Fibrous Scaffolds

Mechanical properties of the MEW fibrous scaffolds were evaluated under uniaxial tensile loading conditions (**Figure 4**), and a nonlinear stress–strain behavior was observed for all scaffolds. When comparing the modulus of the rectangular-shaped scaffolds in direction 1 (short axis) to direction 2 (long axis), significant increases from 0.70 ± 0.15 to 1.46 ± 0.14 MPa and from 1.18 ± 0.08 to 2.05 ± 0.15 MPa were observed for the Blend40 and PCL scaffolds, respectively (Figure 4d). For the square-shaped scaffolds, no significant difference was observed between the modulus in directions 1 and 2, yielding values from 1.94 ± 0.12 to 2.10 ± 0.14 MPa and 2.40 ± 0.10 to 2.25 ± 0.42 MPa for the Blend40 and PCL scaffolds, respectively. In all cases, the tensile modulus for the Blend40 scaffolds was lower than the correspondent PCL-based scaffolds. This difference likely resulted from the shorter polymer chains of pHMGCL when compared to the PCL polymer. Despite of the relatively inferior tensile properties of the pHMGCL-based scaffolds, the tensile modulus of both polymers is close to the range
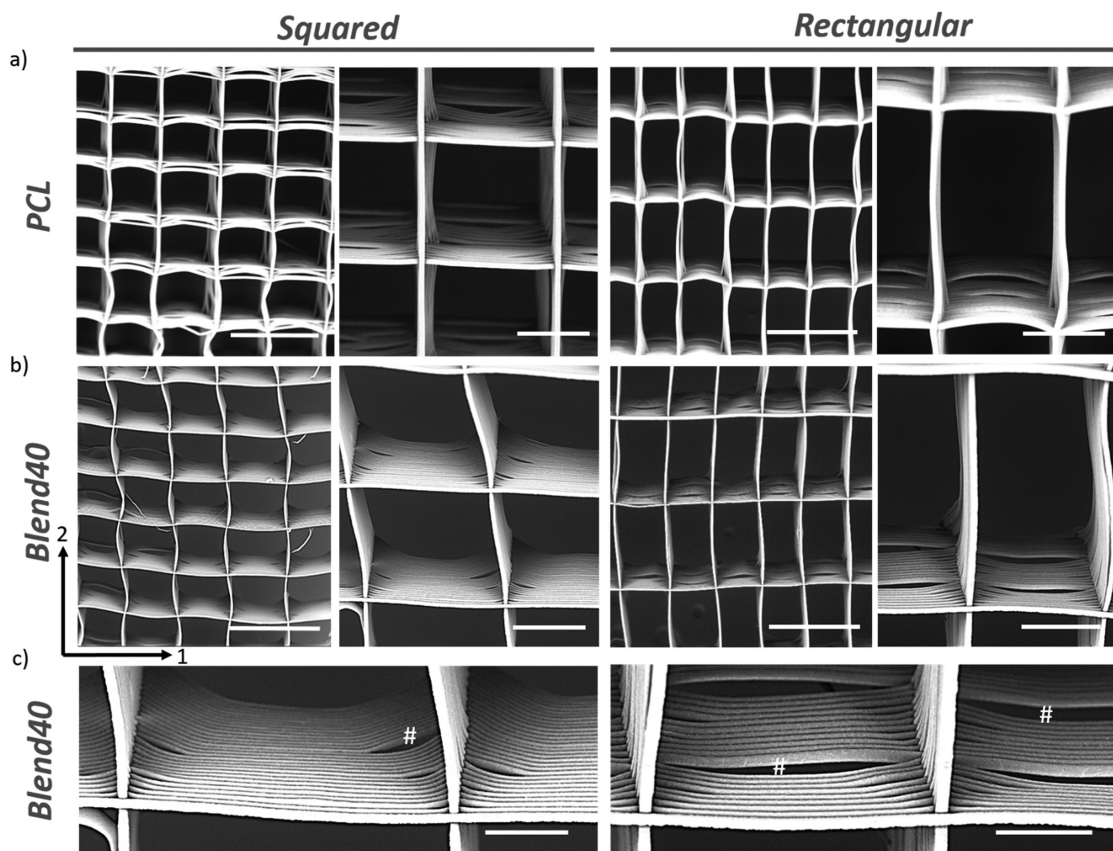
**ADVANCED
SCIENCE NEWS**

www.advancedsciencenews.com

**ADVANCED
HEALTHCARE
MATERIALS**

www.advhealthmat.de

Figure 3. SEM images of the squared and rectangular MEW microfibrous scaffolds prepared from a) PCL and b) Blend40 polymer. Scaffolds were printed with 200 × 200 µm (squared) and 150 × 300 µm (rectangular) interfiber spacing and with a thickness of 400 µm (25–30 layers). Scale bars, 300 µm (low magnification) and 100 µm (high magnification). c) Detailed view of the stacked fibers in Blend40 scaffolds. Local separation of the fiber stacks was observed, creating a porosity between the scaffold compartments (marked with #). A similar effect was observed for PCL scaffolds. Scale bar, 50 µm.

of stiffness reported in the literature for human myocardium[25] To investigate further, the ratio between the tensile modulus in both testing directions was determined for all constructs (Figure 4e). As predicted, the rectangular-shaped scaffolds of both polymer formulations evidenced anisotropic behavior ($E_{T2}/E_{T1} \approx 2$), while the squared ones showed a more isotropic behavior ($E_{T2}/E_{T1} \approx 1$). The aligned fiber scaffolds with a rectangular shape were then found to successfully approximate not only the effective stiffness but also the anisotropic behavior of the native heart tissue.[25,26] It should be noted that only the short-term mechanical properties were evaluated at this stage, and also, it was not evaluated whether these novel constructs interfere with the mechanical functioning of the native tissue surrounding the graft after myocardium implantation.

2.3. Biological Performance

2.3.1. Cell Encapsulation and Viability

To investigate the biological performance, CPCs were combined with a collagen hydrogel and seeded into both the Blend40 and PCL scaffolds. After 7 d, cells were uniformly distributed inside the scaffold, as shown by immunostainings for F-actin

and integrin-β1 (**Figure 5**), with CPCs dispersed throughout the pores and in close contact with the fibers. Cell viability in the scaffolds was assessed with a live/dead staining after 7 d of culture (Figure 5a). In Blend40 scaffolds, very few dead cells were detected with an estimated survival rate of 99.9% and with no distinction seen between the different geometries. In the case of PCL scaffolds, the cell survival rate was also high with an estimated survival rate of around 98%. The high observed cell viability with both materials was to be expected, given the fact that the PCL is already widely used successfully in medical application,[27] and Blend40 is designed as a more cell friendly alternative. A control group of CPCs combined with only the collagen hydrogel was also prepared. However, without the support of the fiber scaffolds, CPCs completely remodeled the collagen matrix into a small clump of tissue within the first 24 h. Therefore, this group was not included for further cell alignment evaluation.

2.3.2. Cell Alignment

The analysis of the nuclear alignment angle and circularity revealed an influence of the scaffold architecture in the cellular arrangement. The squared geometry resulted in a completely
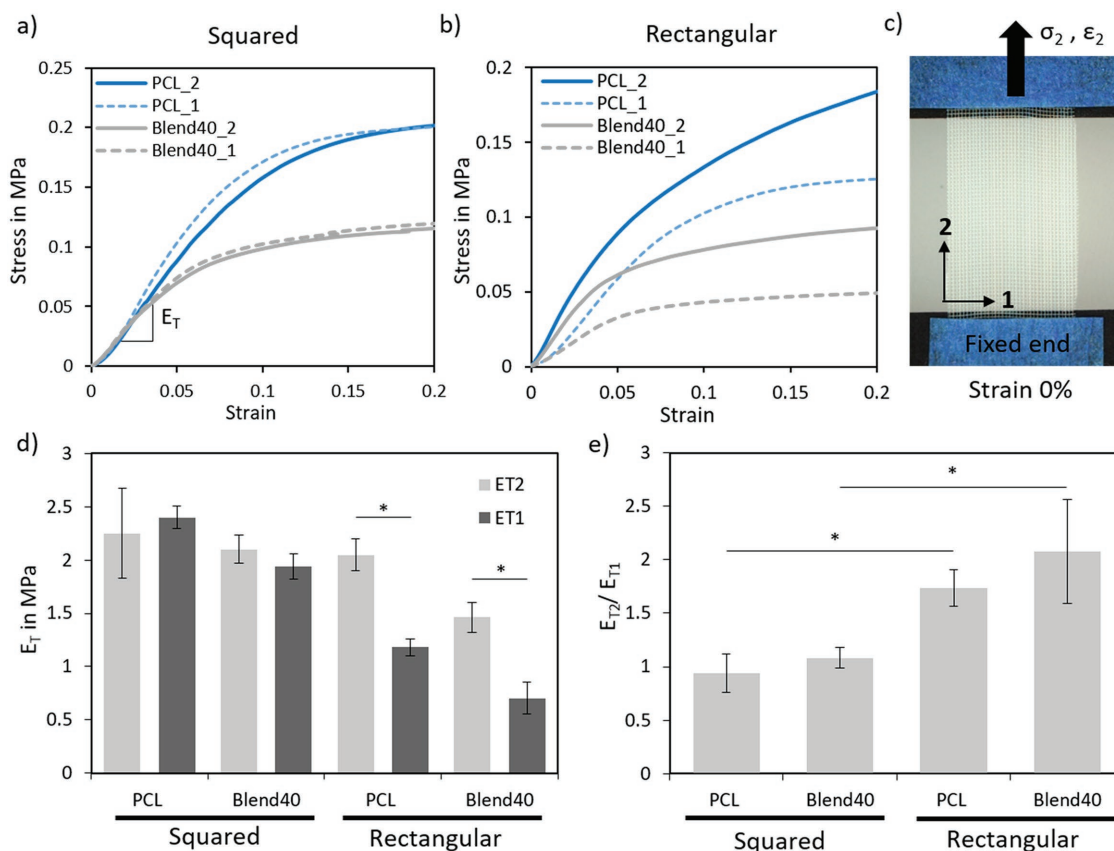
**ADVANCED
SCIENCE NEWS**
www.advancedsciencenews.com

**ADVANCED
HEALTHCARE
MATERIALS**
www.advhealthmat.de

Figure 4. Mechanical properties of prepared MEW fiber scaffolds. Typical engineering stress–strain curve for a) square- and b) rectangular-shaped scaffolds of PCL and Blend40 polymer, when tested under uniaxial tensile test according to the two printing directions, 1 and 2. c) Representative optical image of the sample geometry and fixation grips used for tensile tests. d) Comparison of d) tensile modulus (E_T) in both printing directions and e) tensile modulus ratio between both direction (E_{T2}/E_{T1}) of prepared scaffolds. A probability of error (p) of <0.05 is illustrated with *.

isotropic cellular distribution, with the cells randomly arranged in all directions (Figure 5). The scaffolds with a rectangular architecture, on the other hand, promoted cellular alignment in the preferential direction of the fibers, E_2 (rectangle long axis). Moreover, it was observed that 50% of the cells aligned within 20° in the case of PCL, while 65% of the cells aligned in the Blend40 scaffolds. These results demonstrated a statistical significant difference in cellular alignment between the Blend40 and PCL scaffolds. Similar outcomes were found in the nuclear shape index (NSI), for which CPC's nucleus in the rectangular Blend40 scaffolds was less circular compared to their squared counterparts. It is noteworthy to mention that nuclear alignment can be seen even in the cells far from the fibers (see Figure 5), suggesting that, even though cells sense the fibers at a local level, the Blend40 scaffolds promote organization on a macroscopic scale. Furthermore, CPC's homogenous distribution and alignment throughout the scaffold thickness were confirmed by serial confocal sections at four different depths of a squared PCL scaffold (Figure S1, Supporting Information).

Whereas previous studies have reported limited cell infiltration in fiber scaffolds created by electrospinning,[28] our MEW scaffolds showed a highly porous structure with fully interconnected porosities. The presence of porosity through scaffold walls enabled all compartments to interact (Figure 3C), thereby likely improving CPC cell communication and migration. Nevertheless, these pores show not a clear homogeneity and are not adequately distributed over the scaffold walls. Future studies should address more uniform pore generation within the walls of the fiber scaffolds without compromising accurateness of the fiber stacking. Moreover, the conductivity of the pHMGCL fibers may be improved to allow electrical stimulation as this has been shown to positively influence CPC's behavior.[29] Furthermore, electrical stimulation is suggested for further maturation of potential constructs and to improve the conductance over the construct for the propagation of electrical signals between adjacent cells, especially with the use of contractile cardiomyocytes.

3. Conclusion

In summary, cardiac scaffolds with highly organized fiber architectures were successfully produced by MEW of pHMGCL/PCL blends for the first time. Constructs having a rectangular pattern were found to approximate to the broad mechanical properties of the native myocardial tissue, while, at the same time, promoting CPC's alignment according to the rectangular shape
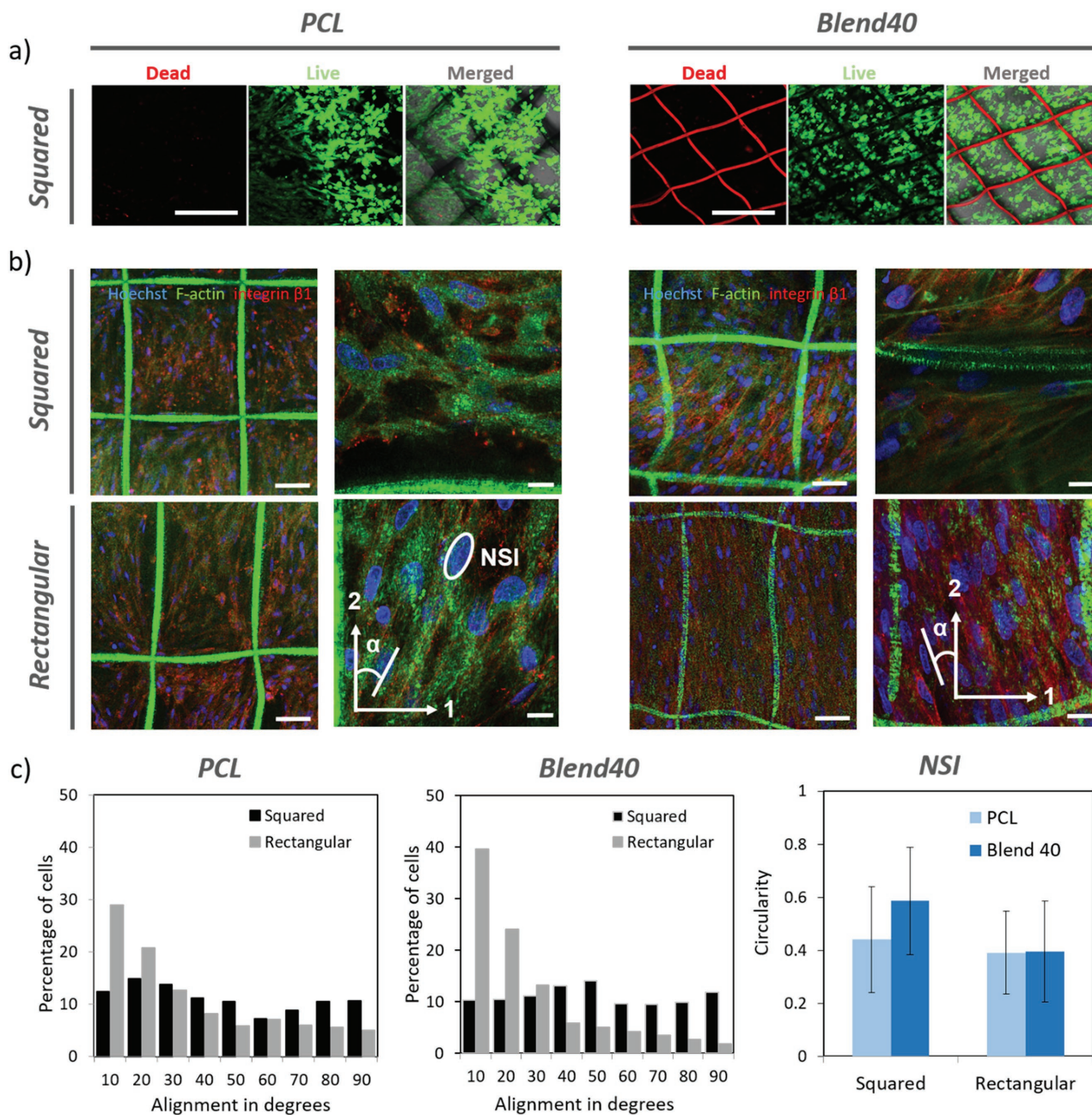
**ADVANCED
SCIENCE NEWS**
www.advancedsciencenews.com

**ADVANCED
HEALTHCARE
MATERIALS**
www.advhealthmat.de

Figure 5. CPC's behavior on the fabricated MEW PCL and Blend40/collagen composite fibrous scaffolds. a) Viability analysis of CPCs 7 d after embedding in PCL and Blend40 MEW scaffolds. In both conditions, seldom dead cells (red) were observed throughout the pores in the scaffold, with ≈98–100% survival rate in all conditions. Scale bar, 250 µm. b) Confocal images of the constructs after 7 d in culture, stained with Hoechst (blue), F-actin (green), and integrin-β1 (red). Scale bar for left images of each polymer composition is 50 µm, whereas for right images is 20 µm. c) Quantification of the CPC's alignment, α, on the scaffolds. Alignment was measured with respect to the vertical microfibers (direction 2), and assumed always positive. Nuclear shape index, NSI, variation as a measure of the circularity of the cell nuclei.

scaffold long axis. Furthermore, the utilization of pHMGCL-based polymer provided a higher degree of cellular alignment in comparison with commonly used PCL polyester. Thus, we envision that our developed approach with enhanced cardiac mechanical and biological relevance can provide a framework for the development of therapeutic viable in vitro cardiac engineered tissues.

4. Experimental Section

Materials: PCL (PURASORB PC 12, Gorinchem, Netherlands) was purchased from Corbion. pHMGCL, was prepared according to the method previously described by Seyednejad et al.[14] Briefly, this hydroxyl-functionalized polyester was synthesized via ring opening polymerization of 3S-benzyloxymethyl-1,4-dioxane-2,5-dione (benzyl protected hydroxymethyl glycolide (BMG)) and ε-caprolactone (monomer

**ADVANCED
SCIENCE NEWS**
www.advancedsciencenews.com

**ADVANCED
HEALTHCARE
MATERIALS**
www.advhealthmat.de

to initiator molar ratio of 300/1) in the melt at 130 °C for 16–24 h, using benzyl alcohol and stannous octoate as initiator and catalyst, respectively. Synthesized polymer was then deprotected to yield the pHMGCL. Blends of pHMGCL/PCL were prepared by mixing both components in a 20:80 and 40:60 weight ratio, and subsequently dissolved in dichloromethane (DCM), to uniformly disperse the two polymers. The solution was stirred at room temperature for 15 min and then the DCM was allowed to evaporate overnight under a flow of dry air. After complete DCM evaporation, solid polymer blends were stored at low temperatures (−5 °C). The chemical structure of the prepared pHMGCL/PCL blends is shown in Figure S2 in the Supporting Information.

Material Characterization: Molecular weights of the raw polymers were measured by GPC on a 2695 Waters Alliance system and a Waters 2414 refractive index detector. Polystyrene standards of known molecular weights were used as standards using AR grade THF as eluent, at the operating conditions of 1 mL min^{-1} and 30 °C. The concentration of the polymers was 5 mL mL^{-1} and injection volume was 50 µL. Thermal properties of the raw polymers and blends were analyzed by DSC on a DSC Q2000 apparatus (TA Instruments, DE, USA). Five milligram of each polymer composition was loaded into an aluminum pan and scanned from −80 to 100 °C with a heating rate of 10 °C min^{-1} and a cooling rate of 0.5 °C min^{-1}, under nitrogen flow. Glass transition temperature (T_g), melting temperature (T_m), and heat of fusion (ΔH_f) were determined. Changes in polymer surface wettability were evaluated by static contact angle measurements using sessile drop technique (Data Physics, OCA 15EC). All measurements ($n = 3$) were performed on uniform polymer films of each composition with a water droplet of 10 µL and repeated in triplicate. Contact angles were measured by averaging the right and left angles of the water droplet using the surface contact angle software (SCA20, Data Physics).

Melt Electrospinning Writing: MEW was performed by a custom-made device as schematically represented in Figure 1. In brief, the device consisted of four principle modules: a dispensing unit, a heating system, an electric field circuit, and a collection setup. The dispensing module contained a disposable glass syringe where the raw polymers and blends were inserted, coupled to one end to a thin metallic nozzle (27G, Unimed Switzerland), and to the other end to a manual pressure regulator (Festo, Germany) operating with air. The heating module was composed of an electrical heating coil element wrapped around the glass syringe and directly connected to a proportional–integral–derivative controller (TR 400, HKEtec, Germany) to control the polymer melting temperature. The electric field was generated by a high voltage (HV) source (LNC 10000, Heinzinger Power supplies, Rosenheim, Germany) between a positive output applied to the syringe nozzle and the grounded planar aluminum collector plate. The plate was driven by an x–y lead screw set-up (Xslide, Velmex, LG-Motion, UK) controlled via an advanced 2-axis stepper motor controller (PMX-2EX-SA, ARCUS Technology Inc., USA).

Parameters Range: Polymer processing compatibility was systematically investigated according to key MEW parameters, specifically the acceleration voltage (U_{acc}), the feeding pressure (p), the collector velocity (v_{col}), and the collection distance (d). Fiber diameter and morphology were investigated by changing the mentioned parameters for the following values: $U_{acc} = [5, 8.5]$ kV, $p = [1, 4]$ bar, $v_{col} = [10, 40]$ mm s^{-1}, and $d = [3, 5]$ mm, one parameter at a time. Several single fibers were printed, at each parameter combination, on microscopic slides placed onto the aluminum collector plate and then examined using a polarized light microscopy (BX51P, Olympus, Japan). The number of fibers used for the diameter measurements was at least $n = 20$. Subsequently, pHMGCL-based scaffolds were manufactured using the following MEW parameters: $U_{acc} = 5$ kV, $p = 2$ bar, $v_{col} = 5$ mm s^{-1}, and $d = 3$ mm, while for the pure PCL scaffolds, the parameters used were $U_{acc} = 7$ kV, $p = 3$ bar; $v_{col} = 25$ mm s^{-1}, and $d = 3$ mm. As control, the real temperature at the MEW syringe was evaluated locally with an handheld thermometer.

Well-organized scaffold meshes (5 × 5 cm^2) having squared (200 × 200 µm) and rectangular patterns (150 × 300 µm) were programmed and fabricated. The final height of every scaffolds was set to ≈400 µm, which conformed with 25–30 layers. During all printings, temperature and relative humidity were kept at 19–21 °C (accuracy ±1 °C) and 35–40% (accuracy ± 5%), respectively. Printed scaffolds were then

visualized using a SEM Phenom Pro (Phenom-World, The Netherlands), at an acceleration voltage of 5–10 kV. Prior to scanning, circular samples with a diameter of 5 mm were cut from the MEW meshes and sputter-coated with a 2 nm layer using a Q150R rotary-pumped sputter (Quorum Technologies, UK). Based on the scaffolds SEM images, the fiber diameter and interfiber spacing were measured by using ImageJ software.

Mechanical Properties: The tensile properties of the fabricated MEW scaffolds were measured on a Q800 DMA (TA Instruments, USA). Tests were performed from 0.01 till 1 N at a constant rate of 0.1 N min^{-1}. Rectangular-shaped samples ($n = 5$) with a length of 10 mm (L_0) and a width of 7 mm (w_0) were cut from each scaffold mesh and attached to a cardboard to ensure a correct alignment and positioning in the tensile grips. The effective elastic modulus, E_T, was calculated from the engineering stress–strain curves at the linear region (i.e., 0–3% strain region), using the following equation

$$E_T = FL_0/\Delta L\, w_0 n_L \varnothing_f \tag{1}$$

where F denotes the applied load, ΔL is the length variation, n_L is the number of printed layers, and $\varnothing_f$ is the fiber diameter. Electrospun scaffolds were tested according to the two directions (1 and 2) of fiber deposition (Figure 4). Their directional-dependent mechanical behavior was quantified by determining the ratio between the effective modulus obtained in both testing directions.

Cell Expansion and Combination with Melt Electrospun Scaffolds: Cylindrical scaffolds of 8 mm in diameter were punched from the electrospun meshes. Prior to cell incorporation, scaffolds were sterilized by soaking them in 70% ethanol for 20 min, followed by a 20-min exposure to ultraviolet light on each side. Human CPCs were obtained and cultured as previously described.[30] To facilitate the cell seeding process, a custom-made mold was used to hold the scaffolds in place. CPCs were suspended in a collagen type I solution and infused into the different scaffolds ($n = 3$) at a concentration of 8×10^6 cells mL^{-1}. Collagen solution was prepared as following, 340 µL Collagen type I (Collagen I rat protein, Thermo Fisher Scientific), 500 µL 2× DMEM, 150 µL PBS, and 10 µL 0.1 M NaOH to balance pH. Constructs were kept in culture for 7 d, after which the whole constructs were either used for a live/dead assay, or fixed in paraformaldehyde for 20 min and kept in PBS at 4 °C until further use.

Cell Viability: The cell viability in the constructs was assessed at day 7 by using a live/dead staining (Live/dead Viability/cytotoxicity kit, Thermo Fisher Scientific, United States), carried out according to the manufacturer's instructions.

Cell Alignment: In order to visualize the cell morphology, stainings for F-actin and integrin-β1 were performed. Briefly, after incubating a primary mouse monoclonal antibody for integrin-β1 (12G10, Santa Cruz Biotechnology, United States) overnight at 4 °C, secondary fluorescent marker (Alexa-Fluor 555, Thermo Fisher Scientific, United States) was added and incubated for 1 h. Afterward, F-actin was stained using marked phalloidin (Fluorescein Phalloidin, Thermo Fisher Scientific, United States). Samples were counterstained with nuclear Hoechst dye for 5 min. Visualization of the samples was performed using a confocal microscope (Leica TCS SP8, Leica Microsystems, Germany), and the images obtained were analyzed using ImageJ software. Built-in functions of ImageJ were used to calculate the nuclear alignment angle and shape index, which were used as a quantitative measure of cell alignment, as previously reported.[31,32] The nuclear alignment angle is defined as the orientation of the major axis of the ellipse that better fits the individual nuclei, and is expressed hereby with respect to direction 2, which corresponds to the direction of the fibers aligned in the vertical direction (long axis of the rectangles, Figure 5). Cells arranged within 10° relative to direction 2 were considered to be aligned, as previously described.[33] The NSI, also known as circularity, was chosen as a measure of the nuclear elongation and subsequently calculated as follows

$$NSI = (Area \times 4 \times \pi)/Perimeter^2 \tag{2}$$

with a value of 1 representing a perfect circular shape.

Statistical Analysis: Statistical analysis of the mechanical parameters and cellular alignment was performed using one-way ANOVA post hoc test (Tukey's test). Differences were considered significant at a probability of error (p) of $p < 0.05$. All data are represented as means ± standard deviations.

Supporting Information

Supporting Information is available from the Wiley Online Library or from the author.

Acknowledgements

Conflict of Interest

The authors declare no conflict of interest

Keywords

[1] M. A. Laflamme, C. E. Murry, *Nature* **2011**, *473*, 326.

[2] D. A. M. Feyen, R. Gaetani, P. A. Doevendans, J. P. G. Sluijter, *Adv. Drug Delivery Rev.* **2016**, *106*, 104.

[3] R. Madonna, L. W. Van Laake, S. M. Davidson, F. B. Engel, D. J. Hausenloy, S. Lecour, J. Leor, C. Perrino, R. Schulz, K. Ytrehus, U. Landmesser, C. L. Mummery, S. Janssens, J. Willerson, T. Eschenhagen, P. Ferdinandy, J. P. Sluijter, *Eur. Heart J.* **2016**, *37*, 1789.

[4] K. Zhu, S. Shin, T. Kempen, Y. Li, V. Ponraj, A. Nasajpour, S. Mandla, N. Hu, X. Liu, J. Leijten, Y. Lin, M. Asif Hussain, Y. Zhang, A. Tamayol, A. Khademhosseini, *Adv. Funct. Mater.* **2017**, *27*, 1605352.

[5] R. Gaetani, D. A. M. Feyen, V. Verhage, R. Slaats, E. Messina, K. Christman, A. Giacomello, P. A. F. M. Doevendans, J. P. G. Sluijter, *Biomaterials* **2015**, *61*, 339.

[6] J. Groll, T. Boland, T. Blunk, J. A. Burdick, D. Cho, P. Dalton, B. Derby, G. Forgacs, Q. Li, V. A. Mironov, L. Moroni, M. Nakamura, W. Shu, S. Takeuchi, G. Vozzi, T. B. F. Woodfield, T. Xu, J. J. Yoo, J. Malda, *Biofabrication* **2016**, *8*, 013001.

[7] M. Kitsara, O. Agbulut, D. Kontziampasis, Y. Chen, P. Menasché, *Acta Biomater.* **2017**, *48*, 20.

[8] D. Kai, M. Prabhakaran, G. Jin, S. Ramakrishna, *J. Biomed. Mater. Res. B Appl. Biomater.* **2011**, *98*, 379.

[9] A. Guex, A. Frobert, J. Valentin, G. Fortunato, D. Hegemann, S. Cook, T. Carrel, H. Tevaearai, M. Giraud, *Acta Biomater.* **2014**, *10*, 2996.

[10] T. Brown, P. Dalton, D. Hutmacher, *Adv. Mater.* **2011**, *23*, 5651.

[11] G. Hochleitner, T Jungst, T. Brown, K. Hahn, C. Moseke, F. Jakob, P. D. Dalton, J. Groll, *Biofabrication* **2015**, *7*, 035002.

[12] G. Hochleitner, J. F. Hümmer, R. Luxenhofer, J. Groll, *Polymer* **2014**, *55*, 5017.

[13] T. Brown, P. Dalton, D. Hutmacher, *Prog. Polym. Sci.* **2016**, *56*, 116

[14] H. Seyednejad, T. Vermonden, N. E. Fedorovich, R. van Eijk, M. J. van Steenbergen, W. J. Dhert, C. F. van Nostrum, W. E. Hennink, *Biomacromolecules* **2009**, *10*, 3048.

[15] H. Seyednejad, W. Ji, F. Yang, C. F. van Nostrum, T. Vermonden, J. van den Beucken, W. J. A. Dhert, W. E. Hennink, J. A. Jansen, *Biomacromolecules* **2012**, *13*, 3650.

[16] K. Boere, J. Visser, H. Seyednejad, S. Rahimian, D. Gawlitta, M. J. van Steenbergen, W. J. A. Dhert, W. E. Hennink, T. Vermonden, J. Malda, *Acta Biomater.* **2014**, *10*, 2602.

[17] K. Boere, M. M. Blokzijl, J. Visser, J. E. Linssen, J. Malda, W. E. Hennink, T. Vermonden, *J. Mater. Chem. B* **2015**, *3*, 9067.

[18] M. J. Goumans, T. P. de Boer, A. M. Smits, L. W. van Laake, P. van Vliet, C. H. Metz, T. H. Korfage, K. P. Kats, R. Hochstenbach, G. Pasterkamp, M. C. Verhaar, M. A. van der Heyden, D. de Kleijn, C. L. Mummery, T. A. van Veen, J. P. Sluijter, P. A. Doevendans, *Stem Cell Res.* **2007** *1*, 138.

[19] S.-H. Tan, R. Inai, M. Kotaki, S. Ramakrishna, *Polymer* **2005**, *46*, 6128.

[20] G. Hochleitner, A. Youssef, A. Hrynevich, N. Haigh Jodie, T. Jungst, J. Groll, P. Dalton, *BioNanoMaterials* **2016**, DOI: 10.1515/bnm-2015-0022.

[21] T. Brown, A. Slotosch, L. Thibaudeau, A. Taubenberger, D. Loessner, C. Vaquette, P. Dalton, D. Hutmacher, *Biointerphases* **2012**, *7*, 1.

[22] H. Kang, S. Jin Lee, I. Ko, C. Kengla, J. Yoo, A. Atala, *Nat. Biotechnol.* **2016**, *34*, 312.

[23] F. Tian, H. Hosseinkhani, M. Hosseinkhani, A. Khademhosseini, Y. Yokoyama, G. G. Estrada, H. Kobayashi, *J. Biomed. Mater. Res. A* **2008**, *84*, 291.

[24] T. Brown, F. Edin, N. Detta, A. Skelton, D. Hutmacher, P. Dalton, *Mater. Sci. Eng. C* **2014**, *45*, 698.

[25] L. A. Reis, L. Chiu, N. Feric, L. Fu, M. Radisic, *J. Tissue Eng. Regen. Med.* **2016**, *10*, 11.

[26] Q. Chen, A. Bismarck, U. Hansen, S. Junaid, M. Tran, S. Harding, N. Ali, A. Boccaccini, *Biomaterials* **2008**, *29*, 47.

[27] M. A. Woodruff, D. W. Hutmacher, *Prog. Polym. Sci.* **2010**, *35*, 1217.

[28] M. F. Leong, W. Y. Chan, K. S. Chian, M. Z. Rasheed, J. M. Anderson, *J. Biomed. Mater. Res. A.* **2010**, *94*, 1141.

[29] S. Fleischer, M. Shevach, R. Feiner, T. Dvir, *Nanoscale* **2014**, *6*, 9410.

[30] A. M. Smits, P. van Vliet, C. H. Metz, T. Korfage, J. P. Sluijter, P. A. Doevendans, M. J. Goumans, *Nat. Protoc.* **2009**, *4*, 232.

[31] H. Aubin, J. W. Nichol, C. B. Hutson, H. Bae, A. L. Sieminski, D. M. Cropek, P. Akhyari, A. Khademhosseini, *Biomaterials* **2010**, *31*, 6941.

[32] C. T. McKee, V. K. Raghunathan, P. F. Nealey, P. Russell, C. J. Murphy, *Biophys. J.* **2011**, *101*, 2139.

[33] J. L. Charest, M. T. Eliason, A. J. García, W. P. King, *Biomaterials* **2006**, *27*, 2487.